JOURNAL OF GEOPHYSICAL RESEARCH, VOL. 103, NO. D17, PAGES 22,097-22,113, SEPTEMBER 20, 1998

An evaluation of upper troposphere NO_x with two models

Joyce E. Penner,[1] Daniel J. Bergmann,[2] John J. Walton,[1] Douglas Kinnison,[2] Michael J. Prather,[3] Douglas Rotman,[2] Colin Price,[4] Kenneth E. Pickering,[5] and Steven L. Baughcum[6]

Abstract. Upper tropospheric NO_x controls, in part, the distribution of ozone in this greenhouse-sensitive region of the atmosphere. Many factors control NO_x in this region. As a result it is difficult to assess uncertainties in anthropogenic perturbations to NO from aircraft, for example, without understanding the role of the other major NO_x sources in the upper troposphere. These include in situ sources (lightning, aircraft), convection from the surface (biomass burning, fossil fuels, soils), stratospheric intrusions, and photochemical recycling from HNO_3. This work examines the separate contribution to upper tropospheric "primary" NO_x from each source category and uses two different chemical transport models (CTMs) to represent a range of possible atmospheric transport. Because aircraft emissions are tied to particular pressure altitudes, it is important to understand whether those emissions are placed in the model stratosphere or troposphere and to assess whether the models can adequately differentiate stratospheric air from tropospheric air. We examine these issues by defining a point-by-point "tracer tropopause" in order to differentiate stratosphere from troposphere in terms of NO_x perturbations. Both models predict similar zonal average peak enhancements of primary NO_x due to aircraft (≈10-20 parts per trillion by volume (pptv) in both January and July); however, the placement of this peak is primarily in a region of large stratospheric influence in one model and centered near the level evaluated as the tracer tropopause in the second. Below the tracer tropopause, both models show negligible NO_x derived directly from the stratospheric source. Also, they predict a typically low background of 1-20 pptv NO_x when tropospheric HNO_3 is constrained to be 100 pptv of HNO_3. The two models calculate large differences in the total background NO_x (defined as the source of NO_x from lightning + stratosphere + surface + HNO_3) when using identical loss frequencies for NO_x. This difference is primarily due to differing treatments of vertical transport. An improved diagnosis of this transport that is relevant to NO_x requires either measurements of a surface-based tracer with a substantially shorter lifetime than ^{222}Rn or diagnosis and mapping of tracer correlations with different source signatures. Because of differences in transport by the two models we cannot constrain the source of NO_x from lightning through comparison of average model concentrations with observations of NO_x.

1. Introduction

Tropospheric NO_x (= NO + NO_2) plays an important role in determining tropospheric ozone concentrations. Because ozone in the upper troposphere and lower stratosphere is especially effective as a greenhouse gas [*Fishman et al.*, 1979; *Lacis et al.*, 1990], it is important to assess whether concentrations of NO_x in this region may be altered by human activity. Models have demonstrated that the net ozone production rate in this region may increase by roughly a factor of 2 for NO_x increasing from 50 to 200 parts per trillion by volume (pptv) [*Friedl et al.*, 1997].

[1]Department of Atmospheric, Oceanic and Space Physics, University of Michigan, Ann Arbor.
[2]Atmospheric Science Division, Lawrence Livermore National Laboratory, Livermore, California.
[3]Department of Earth System Science, University of California, Irvine.
[4]Department of Geophysics and Planetary Sciences, Tel Aviv University, Tel Aviv, Israel.
[5]Department of Meteorology, University of Maryland, College Park.
[6]Boeing Company, Seattle, Washington.

Paper number 98JD01565.
0148-0227/98/98JD-01565$09.00

NO_x emissions from aircraft are of particular concern for perturbing this region because their emissions are deposited directly into the upper troposphere and lower stratosphere [*Thompson et al.*, 1996; *Friedl et al.*, 1997]. However, the background concentration of NO_x in the upper troposphere is controlled by a variety of other sources: (1) NO_x produced in lightning flashes, (2) NO_x produced in the stratosphere from oxidation of N_2O, and (3) surface-based sources (soil microbial activity, fossil fuel burning, and biomass burning).

Unfortunately, the source strength for lightning NO_x, in particular, is not well constrained. One might hope to constrain it by comparison of predicted NO_x with measurements. Unfortunately, this is not possible because the lifetime for NO_x is short and the available data are sparse [*Emmons et al.*, 1997]. Though comparison with existing data provides some measure of verification, ideally, one would like to also find unique methods to validate the concentration of NO_x from specific sources because the observed total NO_x can be derived from many different combinations of sources. Here we design a model experiment to isolate and hence identify the contribution of individual sources of NO_x in the upper troposphere as well as the role of transport as represented in our two models.

Transport processes affecting the concentrations of NO_x in the upper troposphere/lower stratosphere are represented in

models with considerable uncertainty, in part due to failure to resolve the relevant spatial scales. The highest-resolution chemical transport models in use today are typically T42 (approximately 2.5° × 2.5°), but even models with this resolution cannot resolve the horizontal scales of convection that bring NO_x to the upper troposphere from the surface. Further, they have difficulty representing tropopause fold events [*Rood et al.*, 1992; *Holton et al.*, 1995] that bring stratospheric NO_x and O_3 into the troposphere. Here we use two tracer transport models as examples to define a range in upper tropospheric/lower stratospheric NO_x that results from differences in treating transport in this region. A similar model intercomparison study was recently undertaken by Van *Velthoven et al.* [1997]. Here our results differ, because we consider the role of each source in determining the NO_x concentration and because we use a more realistic treatment of the lifetime for NO_x.

We define our experiment in terms of the major classes of "primary NO_x," for example, NO_x that has not undergone transformation to the longer-lived species HNO_3 (or peroxyacetyl nitrate (PAN)). Source strengths associated with surface-based sources (fossil fuel burning, microbial activity in soils, and biomass burning) appear to be reasonably well defined (Table 1; see also *Lee et al.* [1997]). Likewise the source of total odd-nitrogen ($NO_y = NO_x + HNO_3$ + others, see below) from the reaction of N_2O with $O(^1D)$ in the stratosphere is well defined and thus limits the stratospheric source of NO_x. Current "best guesses" for the lightning source of NO_x, however, differ by more than a factor of 5 with a total NO_x possible range estimated as 1 to 25 Tg N/yr [*Lawrence et al.*, 1995; *Levy et al.*, 1996; *Price et al.*, 1997a, b]. We also examine the contribution to NO_x from "secondary NO_x " derived from in situ photochemical recycling of HNO_3. Concentrations of HNO_3 in the upper troposphere are also poorly constrained by measurement, and current models do a poor job of representing the available data in any case [*Friedl et al.*, 1997]. Below we show that NO_x produced from HNO_3 in the troposphere is small over the range of constrained HNO_3 concentrations from 50 to 200 pptv.

The upper troposphere and lower stratosphere are obviously different regimes in terms of the sources and buildup of NO_x, and to evaluate the effects of aircraft emissions, they must be clearly separated in the model. The chemical lifetime for NO_x in the upper troposphere is 5 to 10 days, comparable to the timescales for venting of boundary layer NO_x via convection and turnover by large-scale air flow. Thus a balance of transport and chemistry determines the distribution of NO_x from different sources here. In the lower stratosphere, timescales for transport are much longer, and a source introduced into this region can build up to concentrations much higher than those in the upper troposphere. Given the longer transport times in the lower stratosphere, the chemistry will approach a steady state between NO_x and the other forms of NO_y. To evaluate the effects of different sources in the upper troposphere and lower stratosphere, it is critical for each model to define the surface below which air is essentially tropospheric and turns over on timescales less than the NO_x lifetime. We term this surface the model's "tracer tropopause" and define it at each time step and location on the basis of simulations of downward moving tracers. This surface does not necessarily correspond to the model's tropopause defined from the temperature lapse rate, but it does accurately separate those regions in the chemical transport model (CTM) where sources may build up and NO_x should be in photochemical steady state from the mixed, non-steady state, multisource environment of the troposphere. The use of this diagnostic allows us to evaluate where emissions specified by pressure altitude, such as aircraft emissions, are introduced in relation to the modeled "tracer tropopause."

In the following we first define our approach, including our simplified treatment of NO_x chemistry, the sources specified in the simulations, and a short description of the models. Section 3 discusses our derivation of the "tracer tropopause" in each model and presents results for the concentration of NO_x derived from the stratospheric source of odd nitrogen. Section 4 shows results derived for the predicted NO_x concentrations from the different tropospheric sources, including the source from recycling of HNO_3. Finally, section 5 presents our conclusions, defining for this pair of CTMs the range of possible upper tropospheric NO_x concentrations associated with transport, lightning, and HNO_3 recycling.

2. Model Description

The experiments described here used the GRANTOUR/ Community Climate Model 1 (CCM1) model [*Penner et al.*, 1991] and the IMPACT model. The latter model is under development as a code capable of using massively parallel computer architectures, and the simulations reported here were run on 64 processors of the Cray T3d. For this study, IMPACT used meteorological fields from the Goddard Data Assimilation Office (DAO) stratospheric model that were interpolated to 25 vertical layers covering the year 1992 [e.g., *Schubert et al.*, 1993] (for another paper using these meteorology fields, see *Weaver et al.* [1996]). The vertical grid is a hybrid coordinate system made up of 11 terrain-following sigma levels (mean pressure levels of 921, 771, 648, 547, 447, 346, 273, 223, 187, 162, and 139 mbars) with an interface at 130 mbars and 14 fixed-pressure levels above (122, 107, 92, 77, 64, 54, 44, 34, 24, 14, 7, 3, 1.4, and 0.63 mbars). The horizontal resolution of this model is 2° by 2.5°. The relatively high vertical resolution in the upper troposphere and stratosphere

Table 1. Sources of NO_x Used in the Model

Source Type	Source Strength	Reference
Aircraft	0.46	*Baughcum* [1996]; *Metwally* [1995]
Fossil fuel burning	21.0	*Benkovitz et al.* [1996]
Biomass burning	6.4	*Liousse et al.* [1996]; *Atherton* [1996]
Soil microbial activity	5.5	*Yienger and Levy* [1995]
Lightning	7.0 (2-12.2)	*Price et al.* [1997a]; *Lawrence et al.* [1995]
HNO_3	5.0	see text
Transport from the stratosphere	0.4	see text

Units are Tg N/yr.

together with the advection scheme of *Allen et al.* [1991] assures a numerically accurate representation of tracer transport in the lower stratosphere and upper troposphere. In particular, the resolution near the tropopause may make this one of the better meteorological models available for assessing the relative importance of stratospheric sources of NO_x to the upper troposphere. Convective mass fluxes were diagnosed for the same year but were taken from the DAO tropospheric model fields (e.g., the GEOS 1 data assimilation system; see *Schubert et al.* [1993]), because convective mass fluxes were not saved during the assimilation process for the stratospheric model. GRANTOUR/CCM1, on the other hand, uses a highly accurate Lagrangian tracer transport scheme, but the basic meteorology driving the model uses a sigma coordinate system with 12 vertical levels (mean pressure levels 991, 926, 811, 664, 500, 355, 245, 165, 110, 60, 25, and 9 mbars) and horizontal resolution of approximately 4.5°×7.5°.

Comparison of model results for ^{222}Rn from this version of the IMPACT model indicates that convection is stronger than that in many other models. Zonal average ^{222}Rn concentrations in July reach 10 x 10^{-21} (vol/vol) in the upper troposphere. These predicted upper tropospheric ^{222}Rn concentrations are larger than simulations of ^{222}Rn that directly use the tropospheric GEOS 1 fields [see *Allen et al.*, 1996, *Allen et al.*, 1997], perhaps because of the differing vertical resolution in the tropospheric and stratospheric assimilations. The cumulus transport scheme in IMPACT was derived from the relaxed Arakawa-Schubert scheme used to generate the GEOS 1 meteorological fields. Within the model the transport is represented by the cloud transport equation,

$$\frac{\partial q_k}{\partial t} = \frac{g}{100}\left\{C_{k+1}\left[Q_{k+1} - q_k\right] - C_k\left[Q_k - q_{k-1}\right]\right\} / \Delta p_k$$

where q_k is the large-scale tracer mass mixing ratio at level k, Q is the tracer mixing ratio within cloud, g is the gravitational acceleration (9.8 m s^{-2}), C is the cumulus mass flux (kg m^{-2} s^{-1}) derived from the GEOS 1 meteorological fields, and p is the pressure in millibars. In these equations, $C_{k+1}Q_{k+1}$ and C_kQ_k are the transport of tracer into and out of the layer k by cloud motions, respectively, while $C_{k+1}q_k$ and C_kq_{k-1} represent the downward transport of tracer by large-scale subsidence compensating for the cloud mass fluxes. This equation is solved iteratively for each time step together with the following equation for Q_k,

$$(C_k + D_k)Q_k = E_k q_k + C_{k+1}Q_{k+1},$$

where E_k and D_k are the rates of entrainment and detrainment of air into the cloud (kg m^{-2} s^{-1}), respectively. Below cloud base, Q_k is set equal to q_k.

Convection in the CCM1 follows a moist adiabatic adjustment scheme [*Manabe and Holloway*, 1975]. The convective mass flux was derived from the vertical exchange of moist static energy that results from the moist adiabatic adjustment, and the following equation for tracer mass was solved [*Walton et al.*, 1988]:

$$\frac{\partial q_k}{\partial t} = \frac{g}{100}(C(k+1/2)/\Delta p_{k+1})q_{k+1} - (C(k-1/2)/\Delta p_k)q_k$$

where the vertical spatial discretization scheme described by *Walton et al.* [1988] has been reversed to use the same notation as that described above for the DAO scheme (i.e., level k+1 is below level k). This equation is solved by using an implicit time discretization. The mass fluxes derived from the CCM1 can be as much as 20 times higher (on average 2 to 4 times higher) than those derived in the GEOS-1 assimilation, but they are applied to grid-averaged mixing ratios rather than to "cloud scale" mixing ratios. Below we show a comparison of these two schemes for an idealized experiment. However, in spite of the differences in their convective mass transport schemes the predicted zonal average upper tropospheric ^{222}Rn concentrations from these two models differ by less than a factor of 2. We note that while the convective mass fluxes developed for the meteorological fields used by IMPACT are more physically based, it is not clear from the radon simulations which of the two schemes is the more realistic. Thus these two models may represent two plausible extremes for vertical and horizontal mixing in the troposphere.

To carry out a model comparison and separate the effects of transport from the effects of chemistry, we have simplified the chemistry of NO_x and NO_y. NO_y in the upper troposphere and lower stratosphere is the sum of NO_x + 2×N_2O_5 + NO_3 + HO_2NO_2 + HNO_3 + $BrONO_2$ + $ClONO_2$ + PAN plus other minor constituents. In the upper troposphere, PAN decomposes very slowly and does not play a major role in the cycling of NO_x versus NO_y, so it is not considered further here. Also, in this region, $BrONO_2$ and $ClONO_2$ are minor components of NO_y and are also ignored as a source of NO_x. The remaining odd-nitrogen compounds (N_2O_5, NO_3, HONO, HO_2NO_2) all interchange with NO_x over the diurnal cycle and are lumped into a single tracer family we define as NO_z. We define the chemistry for NO_z from the rates calculated by the Lawrence Livermore National Laboratory two-dimensional (2-D) model [*Kinnison et al.*, 1994]. The individual reactions diagnosed from the 2-D model that together define the effective loss rates for the family NO_Z are listed below.

$$NO_2 + OH \rightarrow HNO_3$$

$$N_2O_5 \rightarrow 2 \times HNO_3 \quad \text{(aerosol)}$$

$$ClONO_2 \rightarrow HOCl + HNO_3 \quad \text{(aerosol)}$$

$$BrONO_2 \rightarrow HOBr + HNO_3 \quad \text{(aerosol)}$$

$$N_2O_5 \text{ rainout}$$

$$HO_2NO_2 \text{ rainout}$$

One important process that converts NO_z to HNO_3 is hydrolysis of N_2O_5 occurring on wet aerosols. For the 2-D simulation of N_2O_5 hydrolysis we used an aerosol surface area diagnosed from model simulations of sulfate and carbonaceous aerosols in the GRANTOUR model [*Penner et al.*, 1994; *Liousse et al.*, 1996]. Because the aerosol reactions mainly affect the surface-based sources (which are all continental), we used the monthly average aerosol mass concentrations at a latitude associated with mainly continental concentrations of aerosols, i.e., 22°E. The model-derived aerosol mass concentrations were converted to surface area, assuming a lognormal size distribution for ammonium sulfate aerosol that had a mode radius for the dry aerosol of 0.05 μm and a geometric standard deviation of 2.0 [*Kiehl and Briegleb*, 1993]. Carbonaceous aerosol mass from biomass burning, fossil fuel burning, and natural organics was converted to surface area by using a size distribution and composition typical for smoke aerosols [*Chuang et al.*, 1992]. The dry

surface areas for ammonium sulfate aerosol and carbonaceous aerosols were increased by a factor of 2.3 and 1.3, respectively, to account for aerosol growth to an average size at 75% relative humidity. The 2-D rate coefficients, k, were then specified according to

$$k = \frac{1}{4} V \times \mathrm{SAD} \times \gamma$$

where V is the mean molecular velocity, SAD is surface area density, and γ is the reaction probability, taken as 0.1. This expression does not account for gas transport resistance or possible room temperature effects [*Hu and Abbatt*, 1997] that lower the effective value of γ, but sensitivity studies showed that decreasing k by as much as a factor of 10 in the lower troposphere did not have much effect on calculated NO_z in the 2-D model. Thus the overall rate of this reaction is primarily controlled by the rate of the reaction of NO_2 with O_3 to form N_2O_5.

The loss rates developed from the 2-D model in this manner were applied in both 3-D models. Figure 1a shows the reciprocal of the total loss frequency (an e-folding lifetime) as deduced from the 2-D model. Approximately 30% of the total loss rate in the northern hemisphere midlatitude boundary layer in July is through the aerosol/N_2O_5 pathway, decreasing to 20% in the upper troposphere. This pathway accounts for 60% of the loss in the winter hemisphere. We also used the 2-D model to diagnose the ratio of NO_x to NO_z (shown in Figure 1b) for each month. This ratio was used to diagnose NO_x given the predicted zonal average concentrations of NO_z from each 3-D model.

This procedure restricts our calculated NO_x to that obtained from the primary sources without recycling from HNO_3. The secondary source of NO_x from HNO_3 recycling was included separately by diagnosing the loss frequency for HNO_3 photolysis and its reaction with OH to form NO_3 in the 2-D model. This approach allows us to examine the range in background tropospheric NO_x concentrations resulting from uncertainties in concentrations and recycling rates of HNO_3. This scheme differs from that taken in the recent study by *Lamarque et al.* [1996], who tagged each nitrogen-containing molecule from each source of NO_x in their model and allowed feedback between the calculated NO_x, other nitrogen reservoirs, and the odd hydrogen system. Our approach overestimates the increase in NO_x that results from a given increase in source strengths because we have neglected feedbacks between the odd hydrogen abundance and the concentration of NO_x. Figure 2, for example, shows how the lifetime of NO_x varies with NO_x concentration at different altitudes in the midlatitude troposphere. While the dependence is weak in winter, in summer, below about 500 pptv NO_x, the concentration of OH (which mainly determines the lifetime of NO_x) is primarily controlled by the reaction of HO_2 with NO. Thus, in this concentration regime, increases in NO_x sources and concentrations lead to increases in OH, thereby decreasing the lifetime of NO_x. Above the 500 pptv level, further increases in NO_x increase the lifetime of NO_x because the reaction of OH with NO_2 effectively removes odd hydrogen so that OH decreases as NO_x increases. Our linearized chemical scheme will overestimate the sensitivity of NO_x concentration to changes in source strength when NO_x is less than 500 pptv and when recycling from HNO_3 is calculated separately. On the other hand, this simplification allows us to separately explore the effect of recycling and also has the advantage of allowing a direct comparison of the effects of different representations of transport on the NO_x concentration without the complicating influence of changes in the NO_x lifetime. Furthermore, as we show below, model differences in transport can lead to far larger differences than the factor of 2 change in lifetime shown in Figure 2b. A similar linear approach was also used in the study by *Kraus et al.* [1996] and *Köhler et al.* [1997].

Table 1 describes the NO_x sources used in this study together with literature estimates for the range of source strengths considered here for the lightning source. The table also shows the derived source strength from a background concentration of 100 pptv HNO_3. The surface sources noted in the table were input into the lowest model layer for the IMPACT model and into the 1000-900 mbar domain of GRANTOUR. The aircraft emissions used in these calculations are based on air traffic for each month of 1992. Emission inventories of NO_x for both scheduled [*Baughcum et al.*, 1996] and nonscheduled [*Metwally*, 1995] air traffic were combined on a 1° × 1° × 1

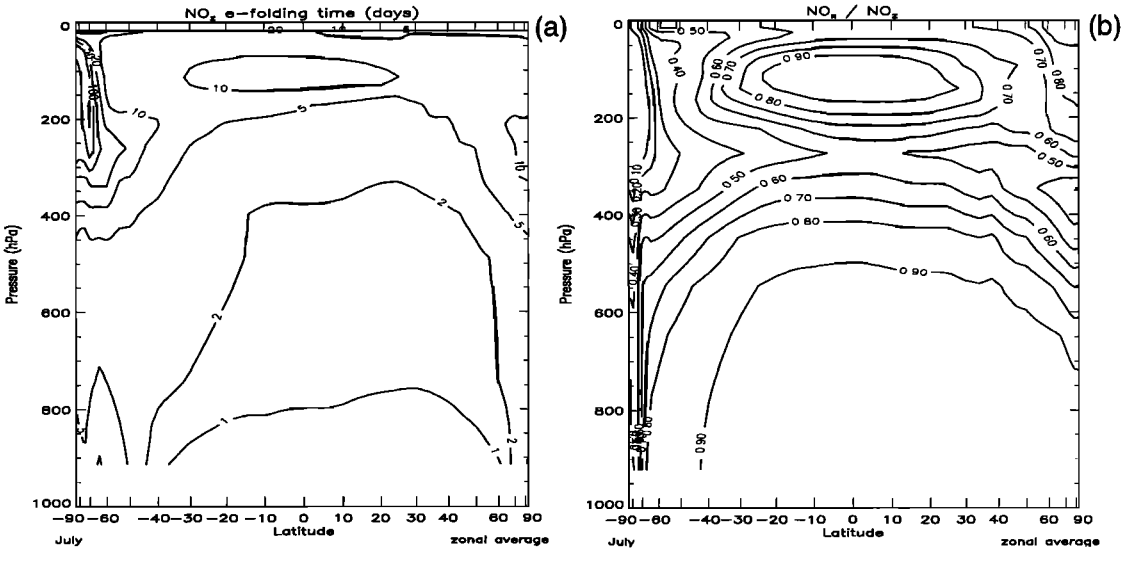

Figure 1. (a) The e-folding lifetime for removal of NO_z (= $NO_x + NO_3 + 2 \times N_2O_5 + HO_2NO_2$) and (b) the ratio of NO_x to NO_z diagnosed from the LLNL 2-D model.

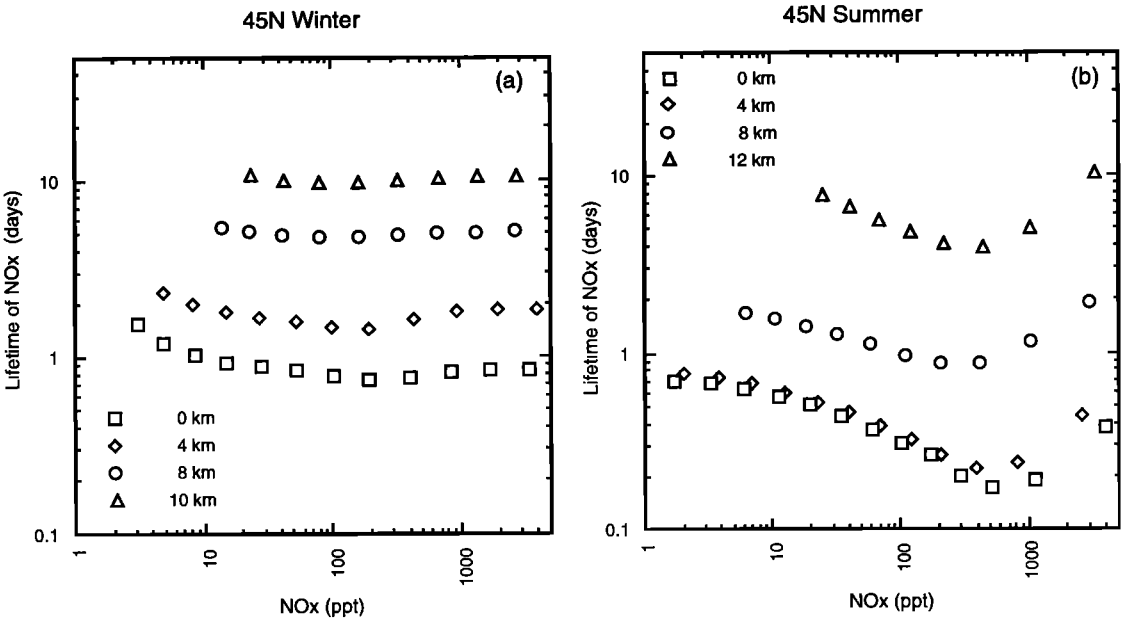

Figure 2. Lifetime of NO_x as a function of NO_x concentration in (a) winter northern midlatitudes and (b) summer midlatitudes.

km (pressure altitude) grid and then interpolated onto the model grids. The lightning sources were developed from monthly mean NO_x production rates per unit surface area as a function of geographic region based on cloud top heights derived by the International Satellite Cloud Climatology Project (ISCCP) and defined at three levels: 115, 245, and 375 mbar [*Price et al.*, 1997a]. Below cloud top, lightning NO_x was distributed with altitude according to an approximate C-shaped profile developed for deep convective events for the tropics, midlatitudes, and oceans (Table 2, from *Pickering et al.* [1996] and K.E. Pickering et al. (Vertical distributions of lightning NO_x for use in regional and global chemical transport models, submitted to *Journal of Geophysical* Research, 1998). Profiles in the table were scaled to the ISCCP cloud top heights. Originally, lightning NO_x was further restricted to levels below the tropopause defined from the temperature profile in

Table 2. Percentage of Mass of NO_x Produced by Lightning as a Function of Altitude for Deep Convective Clouds in Three Regimes

Height, km	Tropical Marine*	Tropical Continental	Midlatitude Continental
0-1	0.7	3.4	21.9
1-2	0.5	1.4	4.4
2-3	0.7	1.5	1.2
3-4	0.7	1.6	1.8
4-5	0.6	1.1	3.5
5-6	0.7	1.3	4.4
6-7	1.3	1.6	3.9
7-8	4.8	2.8	4.7
8-9	12.1	4.6	5.9
9-10	19.2	6.5	7.8
10-11	20.7	8.4	10.3
11-12	19.7	11.0	10.8
12-13	11.5	14.8	9.3
13-14	4.1	17.2	6.6
14-15	1.3	13.6	2.7
15-16	0.5	6.4	0.6
16-17	0.3	2.1	0.1
17-18	0.3	0.6	0.0
18-19	0.2	0.1	0.0
19-20	0.2	0.0	0.0

*All marine sources of lightning NO_x in the model used the "tropical marine" profile developed by *Pickering et al.* [1996] and K.E. Pickering et al., (Vertical distributions of lightning NO_x for use in regional and global chemical transport models, submitted to *Journal of Geophysical Research*, 1998).

each model. However, this procedure sometimes injected NO_x into the a region with largely stratospheric air, and we therefore restricted cloud top lightning NO_x to be below the tracer tropopause defined in section 3.

3. Stratospheric Source of NO_x

We expect that the differentiation between air with substantial concentrations of stratospheric tracers and air with mainly "tropospheric composition" should be represented in the model by a "tracer tropopause." Air parcels above this surface should have longer exchange times with the lower troposphere, while parcels below this level communicate more rapidly with surface and boundary layer air. We have investigated the location of this surface in both GRANTOUR and IMPACT by an idealized experiment in which we injected NO_y into the stratosphere uniformly between 50 mbar and 10 mbar at the rate of 0.4 Tg N/yr and removed it below 800 mbar with a 5-day time constant (case 1) and with a 1-hour time constant (case 2). Regions in which the case 1 and 2 tracers differ by more than 5% clearly define regions that are relatively strongly coupled to the lower troposphere. We define the surface between this model-defined region of tropospheric air and air with substantial stratospheric influence as the "tracer tropopause." This level is approximated in midlatitudes in each model by the 100 pptv stratospheric tracer concentration surface. The use of the 100 pptv surface as a boundary allows us to cleanly define air that has substantial stratospheric influence within the two models. The location of this surface at each grid point is shown in Figure 3 for January 1 for the two models. As Figure 3 shows, this is a highly dynamic surface that changes with longitude as well as time (the vertical range of points with 100 pptv concentration increases by about a factor of 2 if a whole month of data is plotted). The heavy line in this figure and in subsequent figures shows the monthly average model-calculated tracer tropopause in January and July. In the tropics this surface is nearly identical in the two models. North of 40°N in July and north of 30°N in January, however, the GRANTOUR model's tropopause begins to descend more rapidly than that in IMPACT. At the north pole, GRANTOUR has a tracer tropopause level of approximately 400 mbar, while IMPACT has a tracer tropopause level of 300 mbar. It is clear that the effective lifetime for NO_y from aircraft sources that are largest between 200 and 300 mbar and between 40°N and 60°N will differ significantly between the two models as a result of the placement of this source in relation to each model's tracer tropopause. In addition, the contribution of lightning to NO_x could be significantly larger if the source is placed above this level. Similar model differences occur in the southern hemisphere poleward of 30° latitude.

We note that the choice of the 100 pptv level of stratospheric NO_y tracer as a surrogate for the 5% difference level between our two tracer experiments is significantly smaller than the concentration of NO_y normally associated with the physical tropopause (defined by the level above 500 mbar at which the lapse rate becomes smaller than 2°K km^{-1}), and in fact, our 100 pptv level lies below each model's average physical tropopause in midlatitudes. We note that the physical tropopause shows similar scatter about the average, similar to our 100 pptv level. According to observations, the average value of NO_y near the physical tropopause is close to the 500 pptv concentration level but may vary between 200 and 800 pptv [*Murphy et al.*, 1993]. Data presented by *Murphy et al.* [1993] also show a decrease to an average value of 250 pptv within 500 m of the physical tropopause (see Figure 10 of that paper). In both models we find that the zonal mean 250 pptv NO_y contour in midlatitudes approximates the zonal mean physical tropopause, while the 500 pptv level is above the average physical tropopause in midlatitudes.

A number of reasons may explain why our model-derived tracer tropopause NO_y value does not agree with the 500 pptv level of *Murphy et al.* [1993]. First, we are measuring the surface that describes reasonably fast (5 to 10 days) communication with air below 800 mbar, a surface that describes where sources may build up in the model to concentrations higher than those they would attain within the lower troposphere. Second, even our high-resolution model, IMPACT, has a vertical resolution in this region of only about 1500 m. Thus it is perhaps remarkable that the models are able

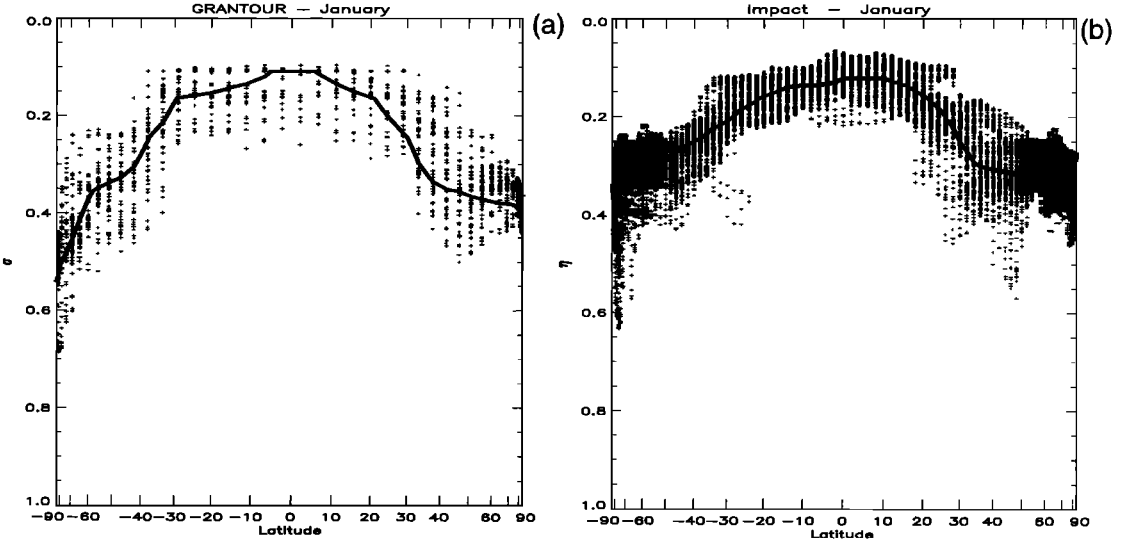

Figure 3. Instantaneous vertical location of the 100 pptv contour on January 1 for the stratospheric tracer experiment defined in section 3 for (a) GRANTOUR and (b) IMPACT.

to come within a factor of 2 of the value of NO_y at the physical tropopause, given that real atmospheric concentrations may change by that much in only 500 m. Thus numerical diffusion may be causing the concentrations in our modeled tracer-tropopause to be less than they would be in a higher-resolution model. Third, if one examines plots of NO_y, O_3, or their ratio when plotted against pressure level (as we do approximately, by plotting NO_x results in sigma and eta coordinates), the features seen in the plots may not precisely correspond to features seen in data when plotted as distance from the physical tropopause. For example, Figure 6 of *Murphy et al.* [1993] shows that NO_y/O_3 is approximately constant above about 100 mbar in midlatitudes and is equal to 0.003, but NO_y/O_3 increases to 0.007 at 300 mbar, a level consistent with an average of 100 ppbv O_3 (the value usually associated with the tropopause). Thus the level that one might associate with the tropopause on the basis of the O_3 concentration has a NO_y/O_3 ratio outside the range usually considered "stratospheric." Clearly, local variability in the pressure level of the physical tropopause can make analysis of precise concentrations of tracers difficult in this coordinate. Finally, it is possible that lightning-produced NO_y in the upper tropical troposphere could enter the tropical stratosphere, supplying the lower stratosphere with more NO_y than one would calculate in a model experiment that includes only the stratospheric source. This NO_y would be a minor component of total NO_y at higher altitudes in the stratosphere but may contribute to the concentration of NO_y at the tropopause.

The model study undertaken here must differentiate between primary NO_x as that which is directly input from a given source and secondary NO_x as that which is recycled from HNO_3 (other sources such as PAN, as noted above, are not important in the upper troposphere and are not included). This problem is not easily formulated with respect to the stratospheric source of primary NO_x, since most NO_y in the stratosphere is HNO_3 and less than 10% enters the troposphere as primary NO_x. We present a new approach here that clearly separates primary and secondary NO_x from the model stratosphere. As we noted above, the "tracer tropopause" is associated with air having greater than 100 pptv of stratospheric NO_y in both models. Therefore, in our simulations of the stratospheric source of primary NO_x, we defined all air that had a stratospheric $NO_y > 100$ pptv as "stratospheric." Within this region of the model, both NO_z and HNO_3 were carried as prognostic variables, so that NO_z formed HNO_3 with a time constant defined by the 2-D model (i.e., by the reactions that form HNO_3) and HNO_3 was recycled back to NO_z with a time constant defined by the photolysis of HNO_3 and its reaction with OH as diagnosed from the 2-D model. When NO_y (= NO_z + HNO_3) was below 100 pptv, we followed the procedure outlined in section 2 for the tropospheric sources of NO_x, namely, NO_z was removed at the local rate determined from the 2-D model (Figure 1a) and there were no other sources of NO_z (no recycling from HNO_3 to NO_x, which is treated separately; see section 4).

Figure 4 shows the zonal average concentrations of primary stratospheric NO_x from the GRANTOUR and IMPACT models. This figure demonstrates that mixing of this stratospheric tracer below the tracer tropopause is, at least at northern midlatitudes, surprisingly similar in the two models. A strong downward mixing near 30°N is evident in the IMPACT model, especially in July. We note that the stratospheric NO_x mixing ratios appear quite flat in both models throughout the tropical upper troposphere, a region normally associated with upward movement of air. The GRANTOUR mixing ratios in January even appear consistent with a downward moving source in this region. The flat contours in the tropical upper troposphere are associated with horizontal mixing in both models. To investigate the source of the apparent downward movement of tracer in the January simulations in GRANTOUR, we performed a model experiment in which all mixing processes within GRANTOUR were turned off. Thus the only transport was that due to large-scale advection. The appearance of the source near the tropical tropopause was diminished because downward and horizontal transport by mixing was zeroed, but the feature was still present at lower altitudes. We compared these features with the zonal average vertical velocities from the model. This comparison showed that the apparent downward moving source in the tropics is actually caused by downward motions in the subtropics. This is followed by horizontal advection, which makes it appear (in a zonal average plot) as though the tracer is originating from the stratosphere in downward motion at the tropics, while in fact this downward motion occurs at different latitudes. Similar processes take place in the July simulations but do not exhibit themselves as a possible downward moving stratospheric source in the tropics.

The direct injection of NO_x into the midlatitude troposphere below the tracer tropopause from the stratosphere is quite small in both models. Typically, the free tropospheric values, well away from the tracer tropopause, are less than 5 pptv. The most abundant form of NO_y from stratospheric injection, however, is predicted to be HNO_3, with typical concentrations of 20 to 50 pptv in the free troposphere in both models (not shown). HNO_3 concentrations as large as 100 pptv could only produce an additional 5-10 pptv of NO_x in the troposphere, as is shown along with the other NO_x sources in section 4. Therefore the total NO_x concentration due to stratospheric sources (i.e., derived from a combination of direct NO_x transport and HNO_3 chemical conversion to NO_x) is at most of the order of 20 pptv below the tracer tropopause. Above the tracer tropopause the total NO_x was calculated from the exchange with HNO_3. The values calculated in July north of 45°N and between 200 and 300 mbar are between 5 and 50 pptv in GRANTOUR and between 2 and 50 pptv in IMPACT. They are even smaller in the winter upper troposphere and lower stratosphere. These concentrations are considerably smaller than the measured concentrations of 120-150 pptv NO and 100-300 pptv NO made off the coast of North America during the June 1984 Stratospheric Ozone Experiment (STRATOZ III) [*Drummond et al.*, 1988] and during the January 1991 Tropospheric Ozone Experiment (TROPOZ II) [*Rohrer et al.*, 1997], respectively. They are also far smaller than most the upper tropospheric measurements of NO and NO_x compiled by *Emmons et al.* [1997]. This finding argues against these measured concentrations being explained, on average, by a stratospheric source.

4. Contribution of Tropospheric Sources to Upper Tropospheric NO_x

Figure 5 shows the zonal average concentrations of NO_x for the six tropospheric sources treated here from the IMPACT model in July, while Figure 6 shows those from GRANTOUR. We have superimposed on these graphs the average tracer tropopause from Figure 3. The altitude and magnitude of peak concentrations for both models from the aircraft source (Figures 5a and 6a) are quite similar. Note, however, that the

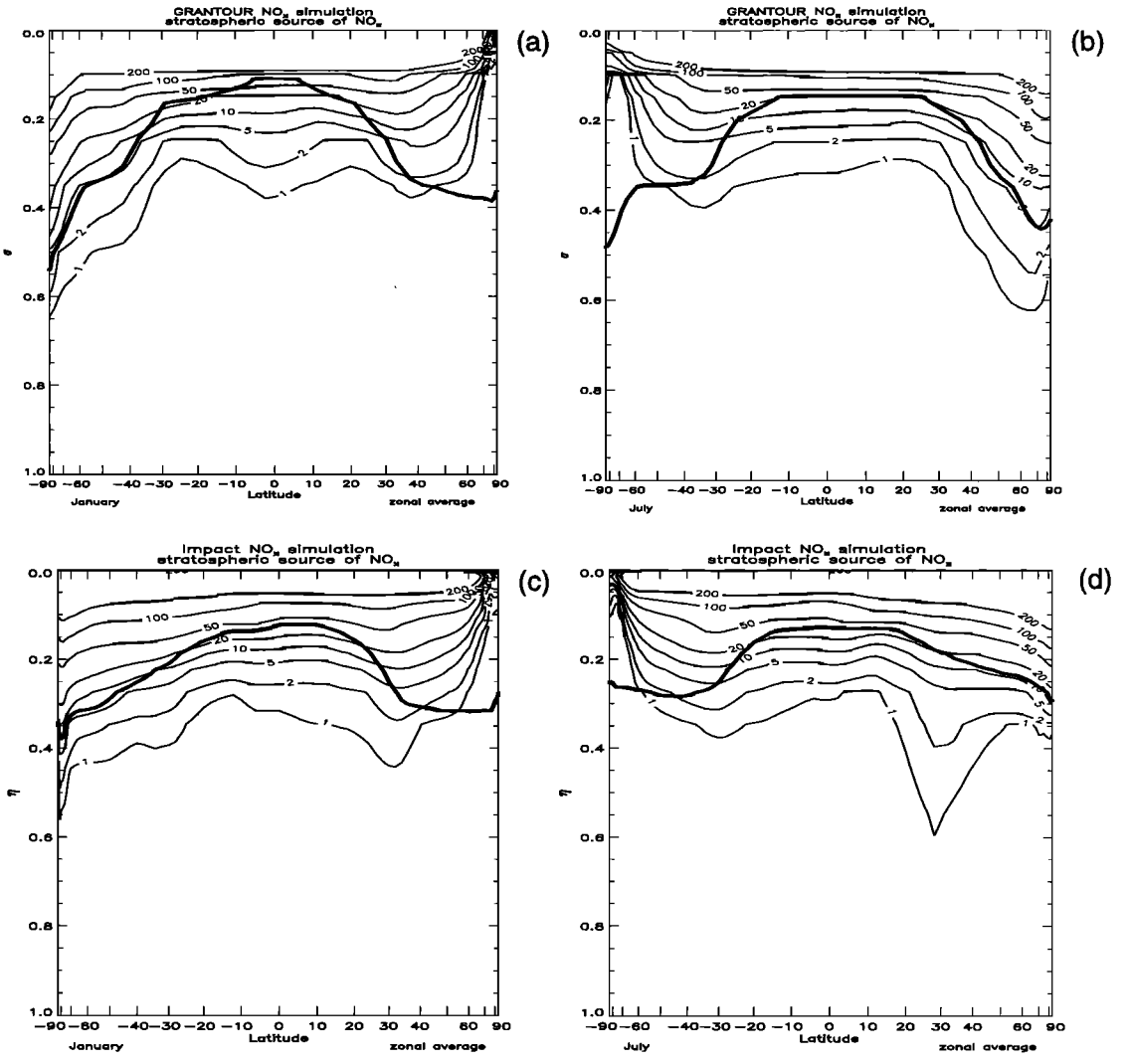

Figure 4. Predicted zonal average primary NO_x mixing ratio from the stratospheric source (pptv) in (a), (c) January and (b), (d) July in the GRANTOUR and IMPACT models, respectively. Superimposed on these plots is the tracer tropopause height in each of the models. The troposphere is defined as the region where the stratospheric tracer concentration was less than 100 pptv.

aircraft source is deposited mainly within the model stratosphere for GRANTOUR, while it is partly in the stratosphere and partly in the troposphere for IMPACT. This difference, together with the more rapid vertical mixing in the IMPACT model, brings NO_x from the upper level source down to the surface more rapidly than happens in GRANTOUR. Consequently, the 5 and 2 pptv concentration contour intervals from aircraft NO_x reach farther into the troposphere in IMPACT in comparison with the same contour intervals in GRANTOUR. Despite this rapid mixing the IMPACT model has a peak zonal average NO_x from aircraft that is >20 pptv, a result of the higher resolution in this model.

Figures 5b and 6b, 5c and 6c, and 5d and 6d depict the zonal mean NO_x concentrations from biomass burning, fossil fuel burning, and the soil source, respectively. The upper tropospheric NO_x concentration from these surface sources are very different in the two models. Thus concentrations in IMPACT reach 20 pptv, 100 pptv, and 50 pptv for the three surface sources in the upper troposphere in July, respectively, while the corresponding concentrations from GRANTOUR are only <1 pptv, 5 pptv, and 2 pptv. In contrast to these differences in the upper troposphere, the surface concentrations are similar in the two models. This large difference in the contribution of surface sources to the upper troposphere was unexpected, since the model-predicted radon concentrations were within a factor of 2. However, NO_z as defined here has a much shorter lifetime at the surface in comparison with radon. The *e*-folding lifetime for radon (5.5 days) allows venting of boundary layer air by convective mixing processes to compete effectively with its chemical removal in both models. Here the *e*-folding lifetime for NO_z is only 1 day near the surface, effectively shutting off vertical transport for the slower overturning in the GRANTOUR model but allowing some emissions to be carried to the upper troposphere in the IMPACT model.

Concentrations of NO_x from lightning (source rate of 7 Tg N/yr) are shown in Figures 5e and 6e. In the upper troposphere, both models predict concentrations reaching 100 pptv. In preliminary simulations we had inadvertently placed the lightning source in the IMPACT model above the tracer tropopause, causing a factor of 2 higher peak zonal average concentrations of NO_x [*Penner et al.*, 1996)]. Here we see that

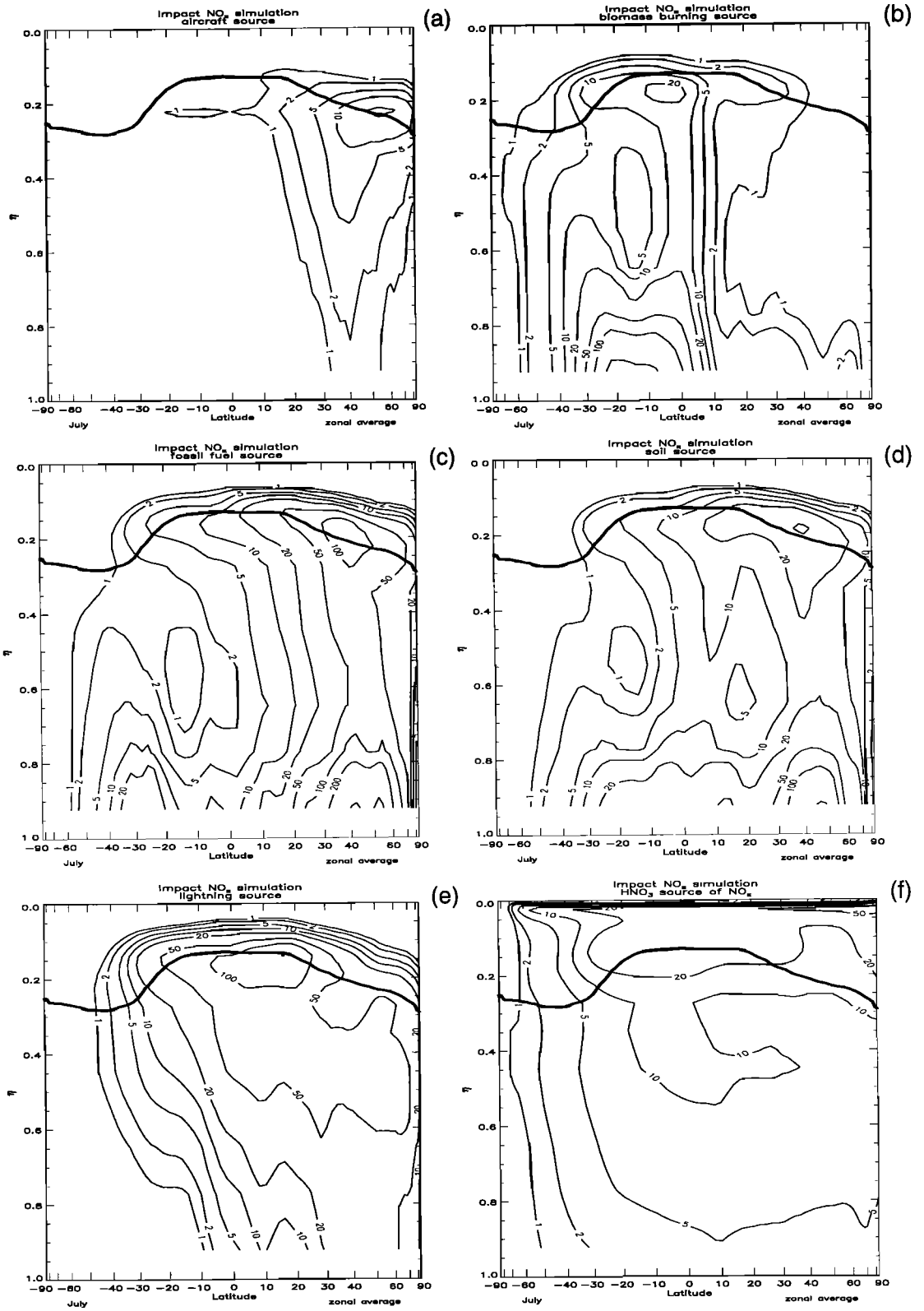

Figure 5. Predicted zonal average NO_x mixing ratio (pptv) in July from the IMPACT model from (a) aircraft, (b) biomass burning, (c) fossil fuel burning, (d) soils, (e) lightning, and (f) the HNO_3 source.

while peak concentrations are similar, just as for the aircraft source, the stronger vertical mixing in IMPACT brings more lightning NO_x toward the surface.

Finally, Figures 5f and 6f show the NO_x concentration that results from the specified background source from HNO_3, assuming a concentration of 100 pptv HNO_3. Again, the most important difference between the two models appears to be the rate of vertical mixing, with NO_x concentrations from HNO_3 penetrating farther toward the surface in IMPACT than in GRANTOUR. It can also be noted that this is a relatively minor

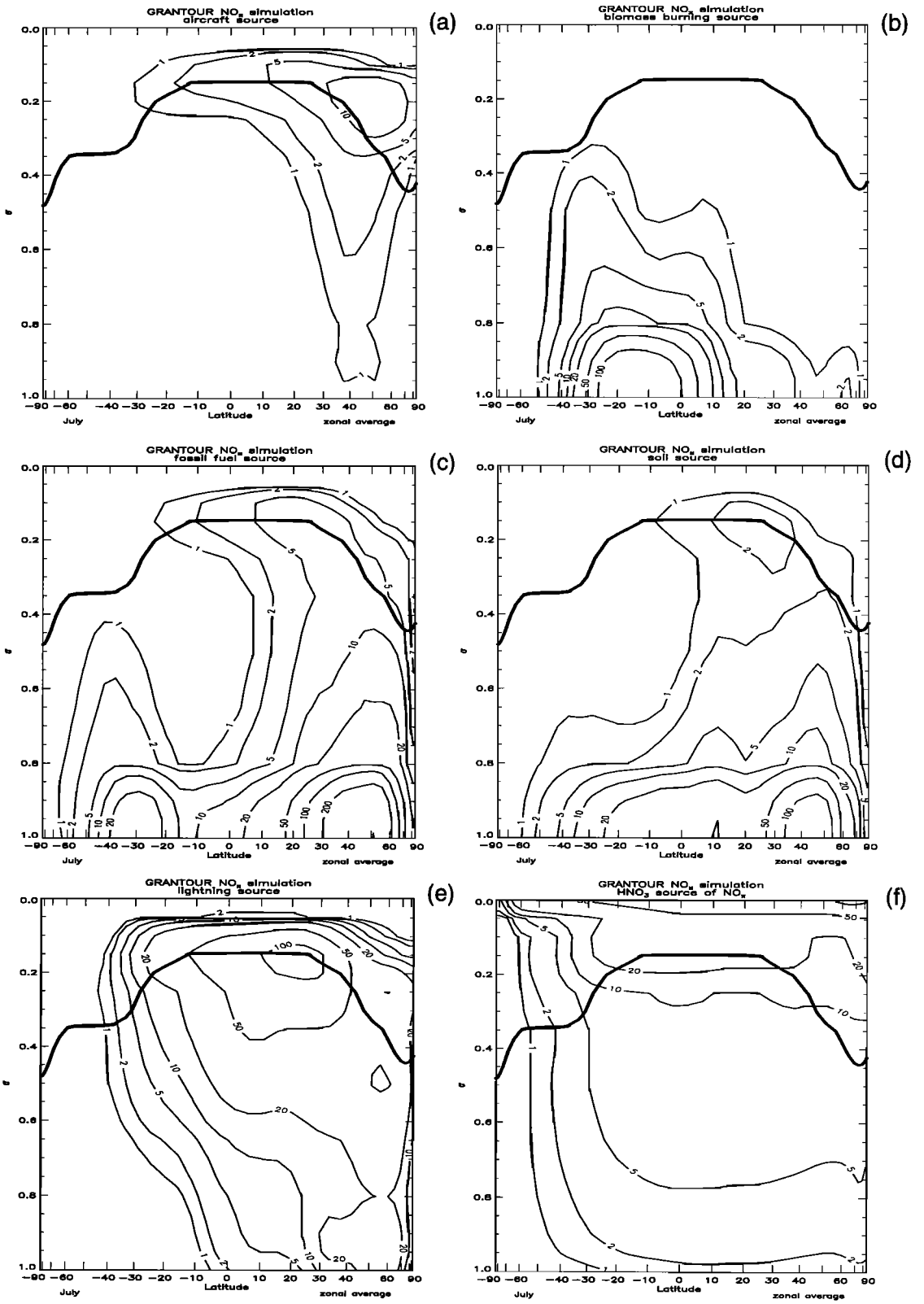

Figure 6. Predicted zonal average NO_x mixing ratio (pptv) in July from the GRANTOUR model from (a) aircraft, (b) biomass burning, (c) fossil fuel burning, (d) soils, (e) lightning, and (f) the HNO_3 source.

source of NO_x in the upper troposphere in comparison with that from lightning in both models or that from fossil fuels in IMPACT. As we noted previously, this background source contributes 5-10 pptv NO_x in the middle latitude upper troposphere and only reaches 20 pptv in the tropical upper troposphere. Thus it is unlikely that upper tropospheric NO_x is largely from the stratosphere.

We investigated the effect of the convective mixing algorithms in the two models with an off-line single-column experiment. In this experiment an initial profile for an

idealized tracer was specified wherein the initial mixing ratio was 1 below a sigma level of 0.74 and zero above that level. We evaluated the mixing ratio after a 48-hour simulation in which the tracer was redistributed according to the convective mixing algorithm in each model. We examined two cases: one in which the lifetime of the tracer was 1 day below the 0.74 sigma level and one in which the lifetime was 5 days below 0.74 sigma. In both cases there was no loss above 0.74 sigma. An idealized convective mass flux profile was assumed in units of kg m^{-2} s^{-1}, which had values of simply the sigma coordinate divided by 100. So, for example, the convective mass flux at 0.58 sigma was 0.0058 kg m^{-2} s^{-1}. The convective mass fluxes between sigma levels of 0.2 to 0.1 were then forced to decrease linearly to zero. There was no mass flux for sigma levels above 0.1. An exact comparison with the model results shown in Figures 5 and 6 is problematic, of course, because the magnitude of the derived convective mass fluxes from the two models differ by up to a factor of 20, but these idealized experiments serve to illustrate what the effect of the two algorithms is. To approximate the effect of different mass fluxes, we applied the algorithm used in GRANTOUR/CCM1, using the same values of convective mass flux, as well as 2 times and 5 times these values. Figure 7 shows the result. The tracer profile developed by using the IMPACT algorithm shows a peak in mixing ratio above the 0.25 sigma level in each case, while the GRANTOUR profiles decrease smoothly for the 5-day tracer lifetime and develop a peak in concentration at lower altitudes in the 1-day tracer lifetime experiment. For larger convective mass flux values the mixing ratios for GRANTOUR increase but never get as high as those predicted with the IMPACT algorithm at the highest altitudes. The redistribution of tracer mass by convection clearly depends also on the initial profile used in this type of experiment. A similar off-line calculation in which the tracer was initially well mixed vertically showed that the GRANTOUR algorithm with 5 times the convective mass flux places more material above the 0.25 sigma level than does the IMPACT algorithm. Figure 7 shows that the schemes in both IMPACT and GRANTOUR can take material from the boundary layer into the free troposphere equally well on a 1-day timescale. The amount actually delivered to the upper troposphere depends on the statistics of convective processes in the models, the magnitiude of the mass flux, and the profiles that develop within the model. Figure 7a, however, demonstrates the fact that the treatment of convection can lead to large differences in upper tropospheric NO_x concentrations if the lifetime of the tracer is only of the order of 1 day. This comparison demonstrates the need to evaluate the model treatment of convection, using a species that is much shorter-lived than the conventional ^{222}Rn to evaluate the model's capability to simulate NO_x.

Figures 8 and 9 show the same results as Figures 5 and 6, respectively, but for the month of January. Concentrations from aircraft are somewhat lower in January than in July. On the basis of chemical removal rates, which are more rapid in summer, we would expect higher concentrations in January. Thus the aircraft NO_x concentrations are most likely controlled by seasonal differences in the dispersion by the meteorological fields together with the seasonal variation in aircraft emissions, which increase by about 30% between 200 and 300 mbar and 40° to 60° N from January to July.

Figures 8b and 9b may be compared with Figures 5b and 6b, respectively, to compare the biomass burning sources in January and July. As these sources are mainly tropical, and both photochemistry and vertical mixing are similar in both seasons in the tropics, the distributions are similar, with July peaks occurring south of the equator and January peaks occurring north of the equator, consistent with the biomass

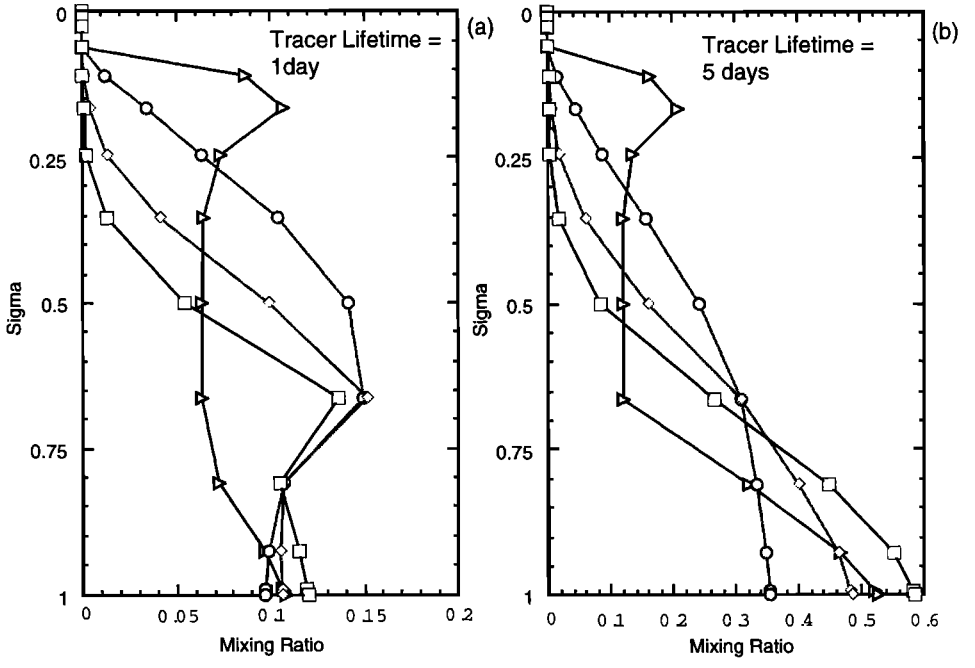

Figure 7. Predicted mixing ratio for an idealized experiment using two convective mixing schemes. IMPACT results are shown by triangles. Squares show the results from the algorithm in GRANTOUR using the same convective mass flux as IMPACT, while diamonds and circles used 2 times and 5 times the mass flux, respectively. The lifetime of the tracer was (a) 1 day and (b) 5 days below the 0.74 sigma level.

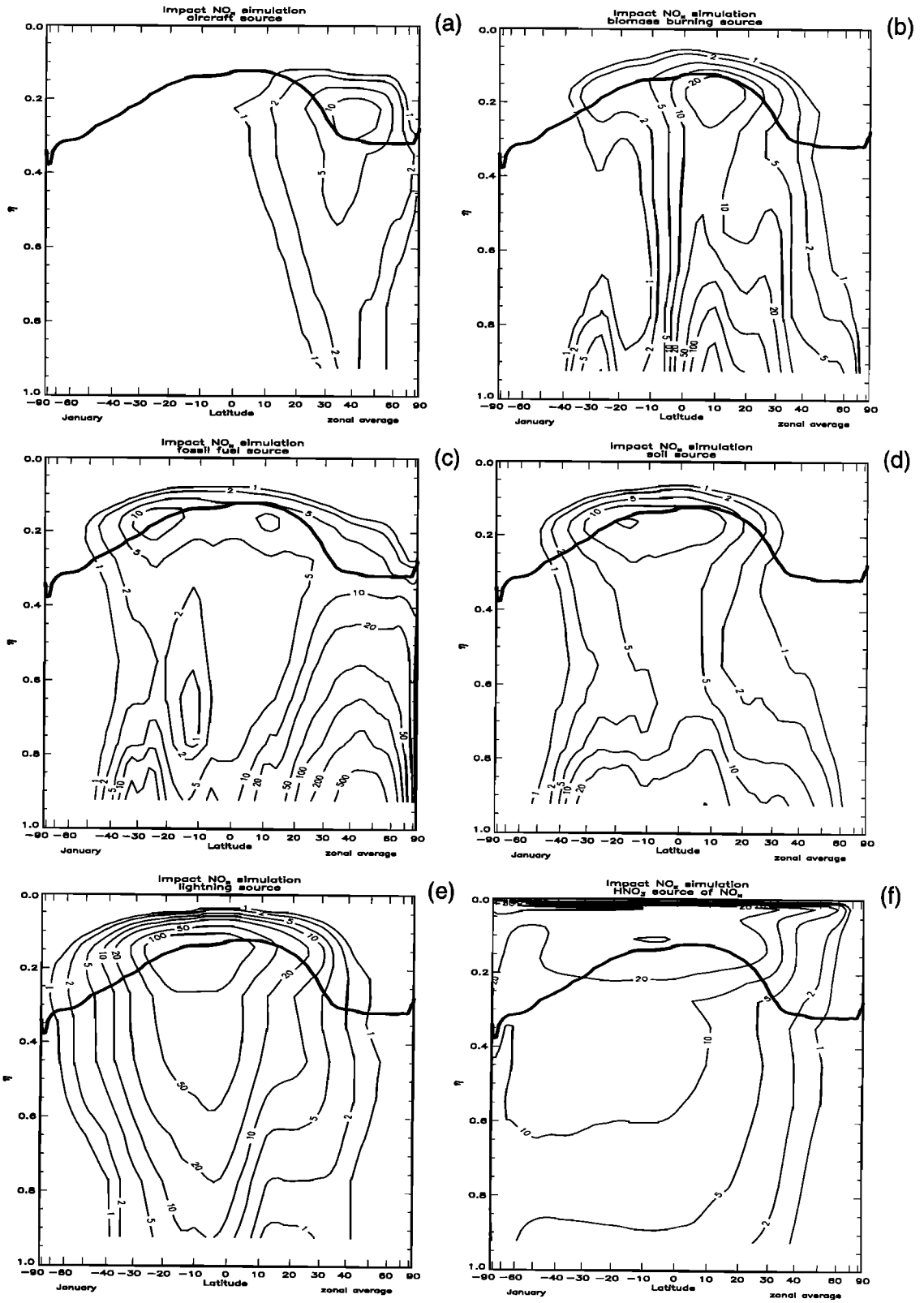

Figure 8. Predicted zonal average NO_x mixing ratio (pptv) in January from the IMPACT model from (a) aircraft, (b) biomass burning, (c) fossil fuel burning, (d) soils, (e) lightning, and (f) the HNO_3 source.

source distributions. The distribution of fossil fuel NO_x, on the other hand, is quite different between the two seasons (compare Figures 8c and 9c with Figures 5c and 6c, respectively). Despite the stronger photochemical removal in July at northern midlatitudes at the surface the strong convection in IMPACT brings peak concentrations of over 100 pptv to the upper troposphere (Figure 5c), while in January (Figure 8c) the concentrations are a factor of 10 lower

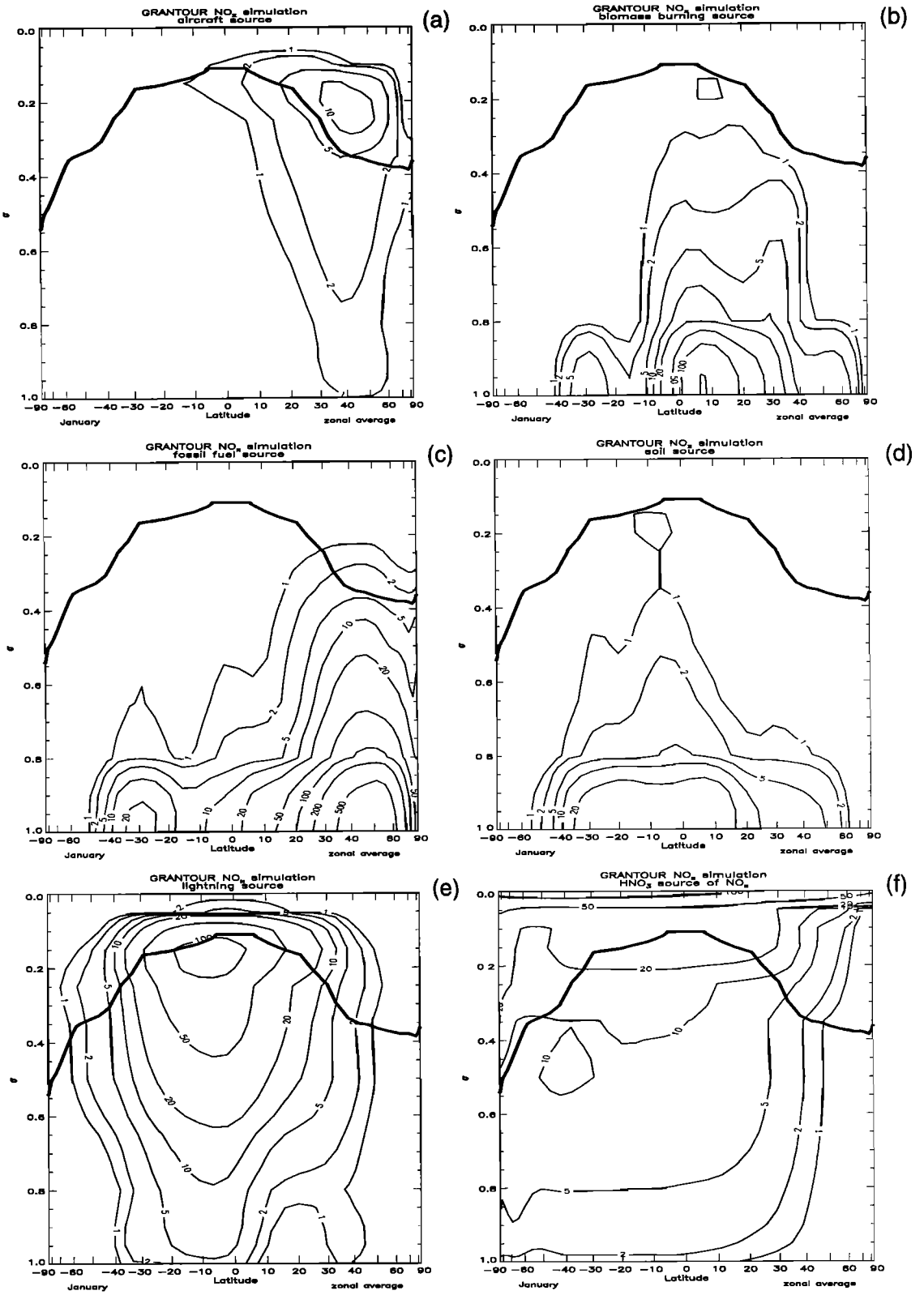

Figure 9. Predicted zonal average NO_x mixing ratio (pptv) in January from the GRANTOUR model from (a) aircraft, (b) biomass burning, (c) fossil fuel burning, (d) soils, (e) lightning, and (f) the HNO_3 source.

at the same altitudes. The slower vertical mixing in the GRANTOUR model does not introduce a large seasonal variation in the resulting upper tropospheric NO_x.

The predicted concentrations from the soil source at northern midlatitudes are higher in July both at the surface and at upper tropospheric levels, reflecting emission rates that are higher in the midlatitude northern hemisphere in summer. The HNO_3 source for January is a near reflection (about the equator) of the source for July, although there appears to be more vertical mixing in January in the southern hemisphere in the

IMPACT model than there is in July in the northern hemisphere. The opposite appears to be the case for the GRANTOUR model (less mixing in the southern hemisphere summer than in the northern hemisphere summer). The distribution of NO_x from lightning is similar in the two seasons except that the stronger source in July in Northern midlatitudes is evident in the large area surrounded by the 50 pptv contour in the IMPACT model and the 20 pptv contour in the GRANTOUR model.

5. Conclusion

The upper and lower limits of total NO_x (all seven sources) in January and July are shown in Figures 10 (IMPACT) and 11 (GRANTOUR). The upper limit assumes 12 Tg N/yr of lightning NO_x and a background of 200 pptv HNO_3, whereas the lower limits assume 2 Tg N/yr of lightning NO_x and 50 pptv HNO_3. In these calculations the source of NO_x from HNO_3 was added below the model's tracer tropopause, while above that level, NO_x from the stratospheric tracer experiment (Figure 4) was used. Both the upper and lower limits constructed for the IMPACT model are considerably higher in the upper troposphere/lower stratosphere than are the upper and lower limits constructed for GRANTOUR. As we noted from our previous examination of different source strengths, this result is mainly due to the stronger vertical mixing present in the IMPACT model and its transport of surface sources. The upper and lower limits for NO_x vary by about a factor of 5 for the GRANTOUR model, while the range is only about a factor of 2 in IMPACT. In keeping with this result the contribution to upper tropospheric NO_x from all anthropogenic sources is much larger in IMPACT (ranging from 40% to 60% in northern midlatitudes in July) than it is in GRANTOUR (10% to 30%).

These simulations demonstrate the large uncertainties associated with prediction of NO_x in the upper troposphere/lower stratosphere. Of the three main determinants of upper tropospheric NO_x (transport, lightning source strength, and recycling from HNO_3) that hamper abilities to predict upper tropospheric/lower stratospheric NO_x, the lightning source strength and vertical transport are of most importance. Predictions of midlatitude upper tropospheric NO_x of the order of 100 pptv in July are

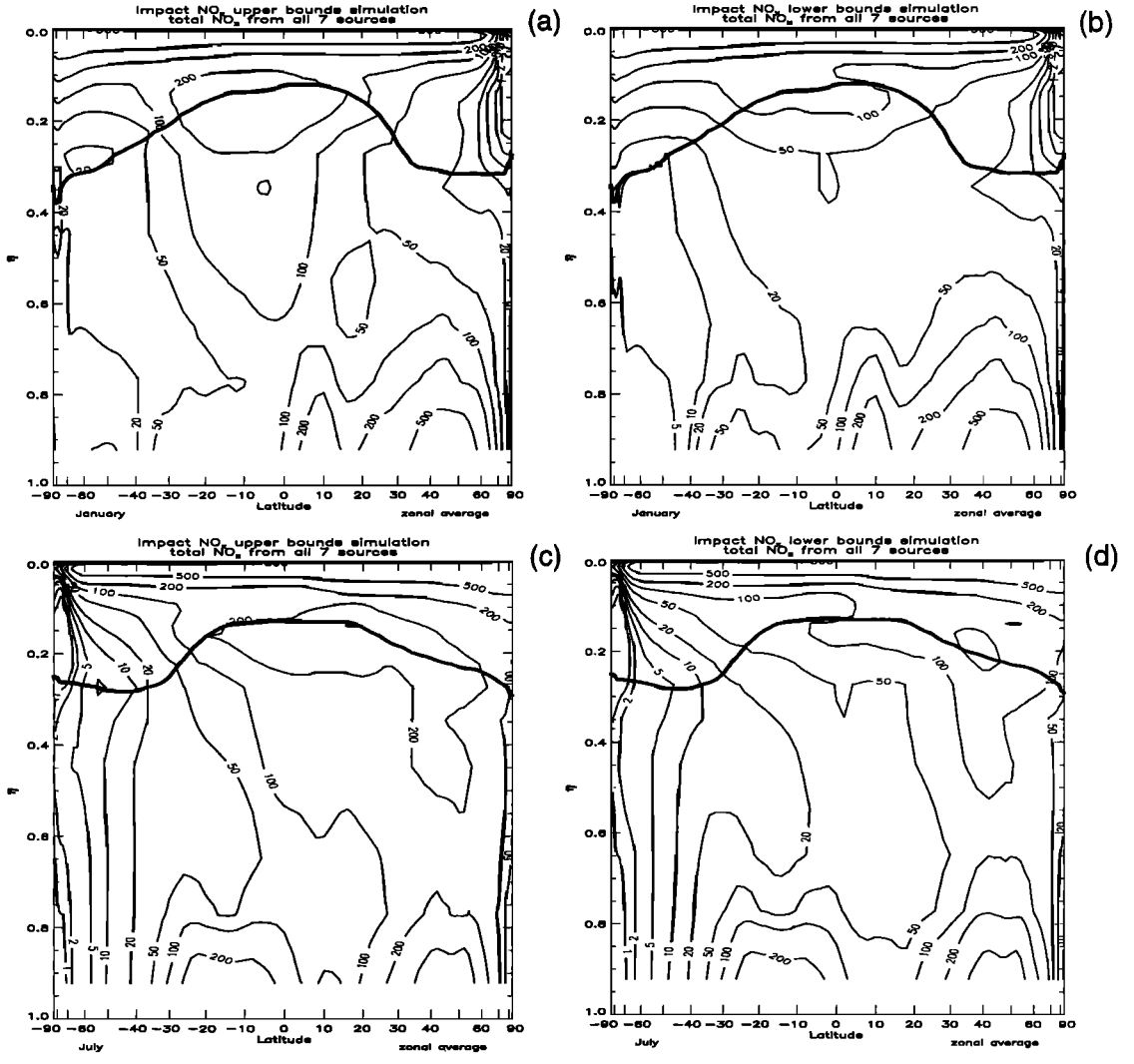

Figure 10. Predicted zonal average NO_x mixing ratio (pptv) in IMPACT in (a), (b) January and (c), (d) July using the upper and lower bounds for lightning (12 and 2 Tg N/yr) and HNO_3 (200 and 50 pptv background concentrations) sources, respectively.

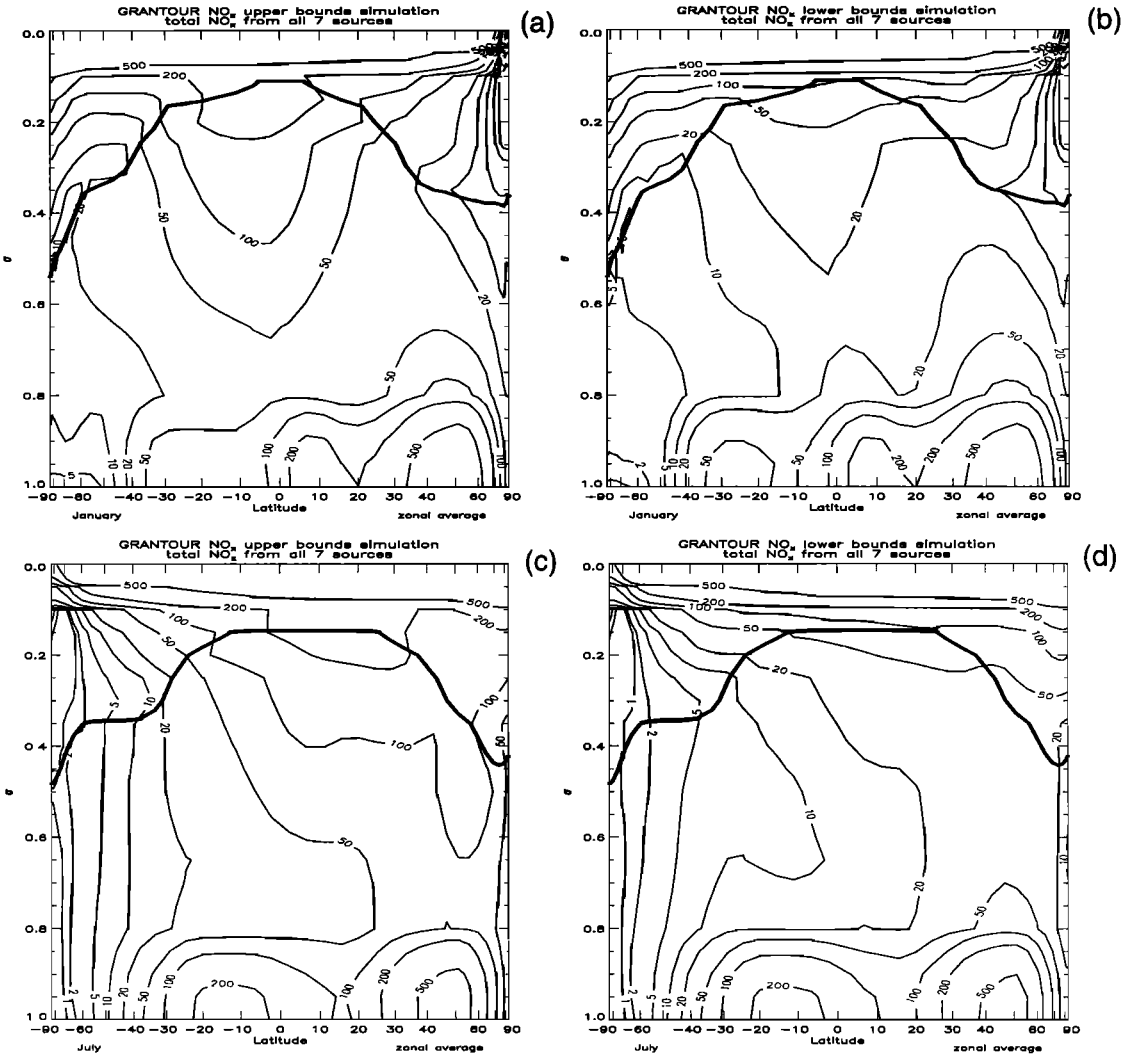

Figure 11. Predicted zonal average NO_x mixing ratio (pptv) in GRANTOUR in (a), (b) January and (c), (d) July using the upper and lower bounds for lightning (12 and 2 Tg N/yr) and HNO_3 (200 and 50 pptv background concentrations) sources, respectively.

consistent with either slow vertical mixing and a large lightning source or more rapid vertical mixing and a smaller lightning source (compare Figures 11c and 10d). Thus, to improve model assessment of ozone change in the upper troposphere/lower stratosphere, it is most important to improve the vertical transport treatment in current models. Further, to test model treatment of convection and vertical transport as it applies to the NO_x problem, it is important either to find a tracer whose lifetime is more similar to that of NO_x or to use methods other than comparison of monthly average model fields with data for testing the models (see below). While this approach is useful for many longer-lived species, comparison of predicted monthly average ^{222}Rn concentrations with data does not provide a sufficiently accurate test for the short-lived NO_x. Comparison of average H_2O and cloud amounts with data (as used by the climate modeling community) would also be insufficiently accurate for testing the transport of short-lived NO_x.

Evaluation of the effects of aircraft emissions present a particularly difficult model challenge. To understand the model response to these emissions, it is very important to understand the model-derived tracer tropopause. Some models may place aircraft emissions entirely within regions with large influence of stratospheric air, while others place them in regions that exchange relatively rapidly with air that has only a 1-day lifetime for NO_x. Entirely different concentration profiles (and perturbations to ambient NO_x and other species) are expected as a result of these differences.

Future verification of any CTM's prediction of tropospheric NO_x and hence O_3 perturbations due to increases in anthropogenic NO_x (e.g., aircraft, surface combustion) requires that each component of NO_x be accurately modeled as well as the total. At present, measurements give us only the total NO_x, and we must rely on model intercomparisons and independent evaluations of individual source strengths to test different CTMs. One method that seems promising, however, is to use NO_x/NO_y as a diagnostic for fresh emissions and correlations of different species with NO_x or NO_y to diagnose the frequency with which air parcels with different sources of NO_x contribute to upper tropospheric air. For example, correlation of NO_y with O_3 and anticorrelation with H_2O can be used to diagnose stratospheric air, and correlations of NO_x with NMHCs, CO or ^{222}Rn can diagnose air that had recently come from surface sources. These tracer/tracer correlations together with

characterization of the ratios of the change in NO_y with change in CO or CO_2 have been used to identify air perturbed by recent aircraft emissions as well as other sources [*Zheng et al.*, 1996]. Testing the ability of models to reproduce such correlation frequencies appears to be one of the more promising methods for gaining confidence in such models and for better quantifying the lightning source.

Acknowledgments. Financial support for this study was supplied by the NASA Atmospheric Effects of Aviation Program. J.E.P. is grateful for support from the DOE Atmospheric Chemistry Program. Computer time was provided by the DOE National Energy Research Super Computing Center.

References

Allen, D.J, A.R. Douglass, R.B. Rood, and P.D. Gutherie, Application of a monotonic upstream-biased transport scheme to three-dimensional constituent transport calculations, *Mon. Weather Rev.*, *119*, 2456-2464, 1991.

Allen, D.J., R.B. Rood, A.M. Thompson, and R.D. Hudson, Three-dimensional radon-222 calculations using assimilated meteorological data and a convective mixing algorithm, *J. Geophys. Res.*, *101*, 6871-6881, 1996.

Allen D.J., K.E. Pickering, and A. Molod, An evaluation of deep convective mixing in the Goddard Chemical Transport Model using International Satellite Cloud Climatology Project cloud parameters, *J. Geophys. Res.*, *102*, 25,467-25,476, 1997.

Atherton, C.A., Biomass burning sources of nitrogen oxides, carbon monoxide, and non-methane hydrocarbons, Rep. UCRL-ID-122583, Lawrence Livermore Nat. Lab., Livermore, Calif., 1996.

Baughcum, S. L. , T. G. Tritz, S. C. Henderson, and D. C. Pickett, Scheduled civil aircraft emission inventories for 1992: Database development and analysis, *NASA Contr. Rep. CR-4700*, 1996.

Benkovitz, C.M., M.T. Scholtz, J. Pacyna, L. Tarrason, J. Dignon, E.C.Voldner, P.A.Spiro, J.A. Logan, and T.E. Graedel, Global gridded inventories of anthropogenic emissions of sulfur and nitrogen, *J. Geophys. Res.*, *101*, 29,239-29,253, 1996.

Chuang, C.C., J.E. Penner, and L.L. Edwards, Nucleation scavenging of smoke particles and simulated droplet size distributions over large fires, *J. Atmos. Sci.*, *49*, 1264-1275, 1992.

Drummond, J.W., D.H. Ehhalt, and A. Volz, Measurements of nitric oxide between 0-12 km altitude and 67°N to 60°S latitude obtained during STRATOZ III, *J. Geophys. Res.*, *93*, 15,831-15,849, 1988.

Emmons, L.K., et al., Climatologies of NO_x and NO_y: A comparison of data and models, *Atmos. Environ.*, *31*, 1851-1903, 1997.

Fishman, J., V. Ramanathan, P.J. Crutzen, and S.C. Liu, Tropospheric ozone and climate, *Nature*, *282*, 818-820, 1979.

Friedl, R.R., et al., Atmospheric effects of subsonic aircraft: Interim assessment report of the advanced subsonic technology program, *NASA Ref. Pub. 1400*, 1997.

Holton, J.R., P.H. Haynes, M.E. McIntyre, A.R. Douglass, R.B. Rood, and L. Pfister, Stratosphere-troposphere exchange, *Rev. Geophys.*, *33*, 403-439, 1995.

Hu, J.H., and J.P.D. Abbatt, Reaction probabilities for N_2O_5 hydrolysis on sulfuric acid and ammonium sulfate aerosols at room temperature, *J. Phys. Chem. A*, *101*, 871-878, 1997.

Kiehl, J.T., and B.P. Briegleb, The relative role of sulfate aerosols and greenhouse gases in climate forcing, *Science*, *260*, 311–314, 1993.

Kinnison, D.E., K.E. Grant, P.S. Connell, and D.J. Wuebbles, The chemical and radiative effects of the Mt. Pinatubo eruption, *J. Geophys. Res.*, *99*, 25,705-25,731, 1994.

Köhler, I., R. Sausen, and R. Reinberger, Contributions of aircraft emissions to the atmospheric NO_x content, *Atmos. Environ.*, *31*, 1801-1818, 1997.

Kraus, A.B., F. Rohrer, E.S. Grobler, and D.H. Ehhalt, The global tropospheric distribution of NO_x estimated by a three-dimensional chemical tracer model, *J. Geophys. Res.*, *101*, 18,587-18,604, 1996.

Lacis, A.A., D.J. Wuebbles, and J.A. Logan, Radiative forcing of climate by changes in the vertical distribution of ozone, *J. Geophys. Res.*, *95*, 9971–9982, 1990.

Lamarque, J.-F., G.P. Brasseur, P.G. Hess, and J.-F. Müller, Three-dimensional study of the relative contributions of the different nitrogen sources in the troposphere, *J. Geophys. Res.*, *101*, 22,955-22,968, 1996.

Lawrence, M.G., W.L. Chameides, P.S. Kasibhatla, H. Levy II, and W. Moxim, Lightning and atmospheric chemistry: The rate of atmospheric NO production, in *Handbook of Atmospheric Electrodynamics*, vol. 1, edited by H. Volland, pp. 189-202, CRC Press, Boca Raton, Fl., 1995.

Lee, D.S., I. Köhler, E. Grobler, F. Rohrer, R. Sausen, L. Gallardo-Klenner, J.G.J. Olivier, F.J. Dentener and A. F. Bouwman, Estimations of global NO_x emissions and their uncertainties, *Atmos. Environ.*, *31*, 1735-1750, 1997.

Levy, H., W.J. Moxim, and P.S. Kasibhatla, A global 3-dimensional time-dependent lightning source of tropospheric NO_x, *J. Geophys. Res.*, *101*, 22,911-22,922, 1996.

Liousse, C., J.E. Penner, C. Chuang, J.J. Walton, H. Eddleman, and H. Cachier, A three-dimensional model study of carbonaceous aerosols, *J. Geophys. Res.*, *101*, 19,411-19,432, 1996.

Manabe, S. and J.L. Holloway Jr., The seasonal variation of the hydrological cycle as simulated by a global model of the atmosphere, *J. Geophys. Res.*, *80*, 1617-1649, 1975.

Metwally, M., Jet aircraft engine emissions database development-1992 military, charter, and nonscheduled traffic, *NASA Contr. Rep. CR-4684*, 1995.

Murphy, D.M., D.W. Fahey, M.H. Proffitt, S.C. Liu, K.R. Chan, C.S. Eubank, S.R. Kawa, and K.K. Kelly, Reactive nitrogen and its correlation with ozone in the lower stratosphere and upper troposphere, *J. Geophys. Res.*, *98*, 8751-8773, 1993.

Penner, J.E., C.S. Atherton, J. Dignon, S.J. Ghan, J.J. Walton, and S. Hameed, Tropospheric nitrogen: A three-dimensional study of sources, distribution, and deposition, *J. Geophys. Res.*, *96*, 959–990, 1991.

Penner, J.E., C.A. Atherton, and T.E. Graedel, Global emissions and models of photochemically active compounds, in *Global Atmospheric-Biospheric Chemistry*, edited by R. Prinn, pp. 223-248, Plenum, New York, 1994.

Penner, J.E., D.J. Bergmann, C. Price, D. Kinnison, J.J. Walton, D. Rotman, M.J. Prather, K.E. Pickering, and S.L. Baughcum, A comparison of lightning and aircraft sources of NO_x in the upper troposphere, paper presented at International Colloquium on Impact of Aircraft Emissions Upon the Atmosphere, Office National D'Etudes Recherches Aerospatiales, Paris, France, Oct. 15-18, 1996.

Pickering, K. E., Y. Wang, W.-K. Tao, and C. Price, The vertical distribution of NO_x produced by lightning (abstract), *Eos Trans. AGU*, *77* (17), Spring Meet. Suppl., S62, 1996.

Price, C., J.E. Penner, and M.J. Prather, NO_x from lightning, 1, Global distribution based on lightning physics, *J. Geophys. Res.*, *102*, 5929-5942, 1997a.

Price, C., J.E. Penner, and M.J. Prather, NO_x from lightning, 2, Using the global electric circuit, *J. Geophys. Res.*, *102*, 5943-5952, 1997b.

Rohrer, F., D. Brüning, and D.H. Ehhalt, Tropospheric mixing ratios of NO obtained during TROPOZ II in the latitude region 67°N-58°S, *J. Geophys. Res.*, *102*, 25,429-25,466, 1997.

Rood, R.B., J.E. Nielsen, R.S. Stolarski, A.R. Douglas, J.A. Kaye, and D.J. Allen, Episodic total ozone minima and associated effects on heterogeneous chemistry and lower stratospheric transport, *J. Geophys. Res. 97*, 7979-7996, 1992.

Schubert, S.D., R.B. Rood, and J. Pfaendtner, An assimilated data set for Earth science applications, *Bull. Am. Meteorol. Soc.*, *74*, 2331-2342, 1993.

Thompson, A. M., R. R. Friedl, and H.L. Wesoky, Atmospheric effects of aviation: First report of the subsonic assessment program, *NASA Ref. Publ. 1385*, 1996.

Van Velthoven, et al., The passive transport of NO_x emissions from aircraft studied with a hierarchy of models, *Atmos. Environ.*, *31*, 1783-1799, 1997.

Walton, J.J., M.C. MacCracken, and S.J. Ghan, A global-scale Lagrangian trace species model of transport, transformation, and removal processes, *J. Geophys. Res.*, *93*, 8339–8354, 1988.

Weaver, C.J., A.R. Douglass, and D.B. Considine, A 5-year simulation of supersonic aircraft emission transport using a three-dimensional model, *J. Geophys. Res.*, *101*, 20,975-20,984, 1996.

Yienger, J.J., and H. Levy II, Empirical model of global soil-biogenic NO_x emissions, *J. Geophys. Res.*, *100*, 11,447-11,464, 1995.

Zheng, J., A.J. Weinheimer, B.A. Ridley, S.C. Liu, G.W. Sachse, B.E. Anderson, and J.E. Collins Jr., Analysis of small- and large-scale

increases of reactive nitrogen observed during the Second Airborne Arctic Stratospheric Expedition, *J. Geophys. Res.*, *101*, 28,805-28,816, 1996.

S. L. Baughcum, Boeing Company, Seattle, WA 98124.

D. J. Bergmann, D. Kinnison, and D. Rotman, Atmospheric Science Division, Lawrence Livermore National Laboratory, Livermore, CA 94550.

J. E. Penner and J. J. Walton, Department of Atmospheric, Oceanic and Space Physics, University of Michigan, 2455 Hayward Street, Ann Arbor, MI 48109-2143. (e-mail: penner@umich.edu)

K.E. Pickering, Department of Meteorology, University of Maryland, College Park, MD 20742.

M.J. Prather, Department of Earth System Science, University of California, Irvine, CA 92727.

C. Price, Department of Geophysics and Planetary Sciences, Tel Aviv University, Tel Aviv 69978, Israel.

(Received April 28, 1997; revised May 4, 1998;
accepted May 7, 1998.)